Structure and Stability Effects of the Mutation of Glycine 34 to Serine in *Rhodobacter capsulatus* Cytochrome c_2[†]

Dezheng Zhao,[‡] Harold M. Hutton,[§,||] Terrance E. Meyer,[§] F. Ann Walker,[⊥] Neil E. MacKenzie,[‡,#] and Michael A. Cusanovich*[,§]

Departments of Biochemistry, Chemistry, and Pharmacology & Toxicology, University of Arizona, Tucson, Arizona 85721

Received December 29, 1999

ABSTRACT: Gly 34 and the adjacent Pro 35 of *Rhodobacter capsulatus* cytochrome c_2 (or Gly 29 and Pro 30 in vertebrate cytochrome *c*) are highly conserved side chains among the class I *c*-type cytochromes. The mutation of Gly 34 to Ser in *Rb. capsulatus* cytochrome c_2 has been characterized in terms of physicochemical properties and NMR in both redox states. A comparison of the wild-type cytochrome c_2, the G34S mutation, and the P35A mutation is presented in the context of differences in chemical shifts, the differences in NOE patterns, and structural changes resulting from oxidation of the reduced cytochrome. G34S is substantially destabilized relative to wild-type (2.2 kcal/mol in the oxidized state) but similarly destabilized relative to P35A. Nevertheless, differences in terms of the impact of the mutations on specific structural regions are found when comparing G34S and P35A. Although available data indicates that the overall secondary structure of G34S and wild-type cytochrome c_2 are similar, a number of both perturbations of hydrogen bond networks and interactions with internal waters are found. Thus, the impact of the mutation at position 35 is propagated throughout the cytochrome but with alterations at defined sites within the molecule. Interestingly, we find that the substitution of serine at position 34 results in a perturbation of the heme β meso and the methyl-5 protons. This suggests that the hydroxyl and β carbon are positioned away from the solvent and toward the heme. This has the consequence of preferentially stabilizing the oxidized state in G34S, thus, altering hydrogen bond networks which involve the heme propionate, internal waters, and key amino acid side chains. The results presented provide important new insights into the stability and solution structure of the cytochromes c_2.

Site-directed mutagenesis offers a powerful means of investigating the relationship of structure and function within families of redox proteins (*1*, *2*). In general, the mutagenesis of redox proteins allows the contribution of individual amino acids to redox properties, protein dynamics, electron-transfer kinetics, protein stability, and function to be investigated (*3*). Within the class I *c*-type cytochromes, which include the mitochondrial cytochromes *c*, the bacterial cytochromes c_2, and other subfamilies, there is considerable structural homology coupled with substantial diversity in amino acid sequence and size (*4*, *5*). In recent years, mutations at structurally equivalent positions have been investigated in class I *c*-type cytochromes, where the amino acid side chain has been conserved throughout evolution (see ref *3* for a relatively recent review). Among the specific positions investigated has been the mutation of proline at position 35 of *Rhodobacter capsulatus* cytochrome c_2 or the structurally equivalent proline at position 30 in eukaryotic cytochrome *c*. The proline at position 35 is of particular interest because there is a hydrogen bond between the ligated histidine $N_\pi H$ and the Pro 35 carbonyl, which is important in orienting the protein backbone with respect to the heme group and which presumably modulates ligand−metal interactions (*6*). Although there is a loss of this conserved hydrogen bond in *Drosophila melanogaster* and rat P35A[1] mutants (*7*), it is still present in *Rb. capsulatus* (*8*), although it has been suggested that the hydrogen bond strength is reduced, which would possibly affect the ligated iron−histidine and iron−methionyl sulfur bonds. Figure 1 presents the three-dimensional structure of reduced *Rb. capsulatus* cytochrome c_2 with a number of key structural features identified.

With both *Rb. capsulatus* cytochrome c_2 and *D. melanogaster* cytochrome *c*, the proline to alanine mutation at position 35/30 destabilized the oxidized cytochrome, consistent with changes in hydrophobicity proximal to the heme (*7*−*9*). Moreover, in the case of *D. melanogaster* cytochrome *c* P30A mutant, the p*K* of the alkaline spectral transition at 695 nm (pK_{695}), which is believed to reflect the stability of the heme iron−methionyl sulfur bond (*10*), is decreased by one pH unit. This is consistent with a 2.3 kcal/mol destabilization of the iron−methionyl sulfur bond (*7*, *9*).

[†] This work was supported in part by a grant from the National Institutes of Health (GM 21277 to M.A.C.) and the Flinn Foundation to the University of Arizona Biological Magnetic Resonance Laboratory.

* To whom correspondence should be addressed. Fax: (520) 621-6603. E-mail: cusanovi@u.arizona.edu.

[‡] Department of Pharmacology and Toxicology.

[§] Department of Biochemistry.

[||] Current address: Chemistry Department, University of Winnipeg, Winnipeg, Canada R3B 2E9.

[⊥] Department of Chemistry.

[#] In memoriam: Neil E. MacKenzie, 1954−1998.

[1] Abbreviations: G34S, substitution of glycine 34 by serine; P35A, substitution of proline 35 by alanine; Gdn-HCl, guanidine hydrochloride.

10.1021/bi992979a CCC: $19.00
Published on Web 03/18/2000

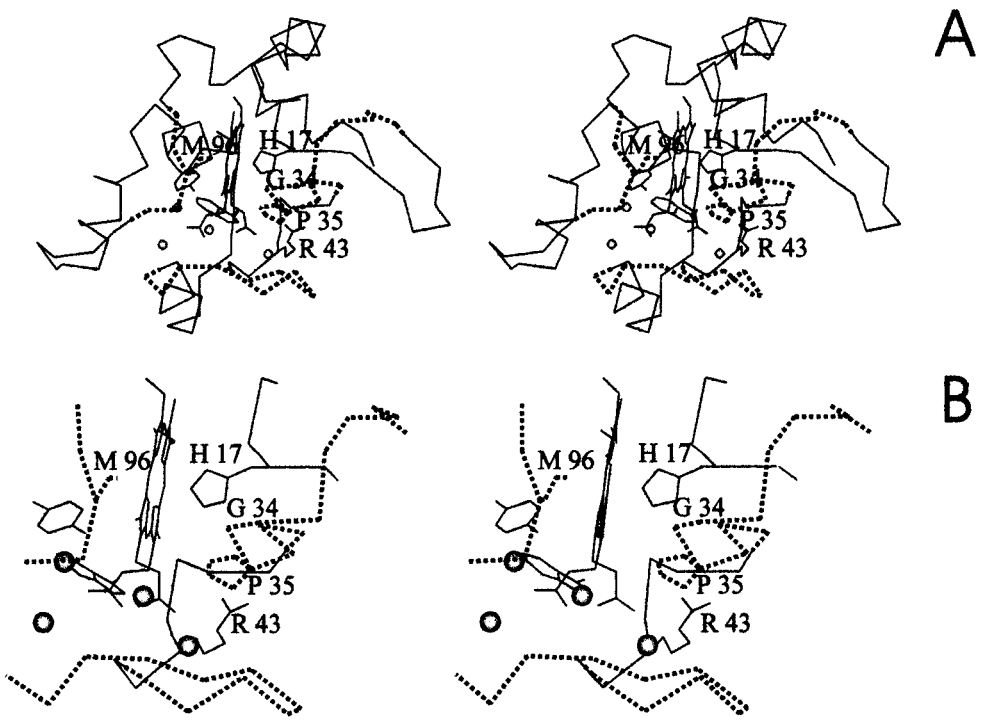

FIGURE 1: Three-dimensional structure of *Rb. capsulatus* ferrocytochrome c_2 (*37*). (A) Backbone and selected side chains. The side chains shown are labeled except for Y75 (left) and W67 (lower left). The waters are shown as spheres and from left to right are 43H, 31H, 45H, and 18H (in the rear in stereo). Dashed lines are backbone regions 94−98 (left), 46−56 (bottom), and 27−36 (right). (B) Expanded view of key structural features. Features are identified as in part A.

However, in the case of the *Rb. capsulatus* cytochrome c_2 P35A mutant, the alkaline pK_{695} is unaltered (*6*, *8*). Thus, mutations at positions which are conserved in both the chemistry of the amino acid side chain and the tertiary structure can have quite distinct effects in homologous cytochromes.

Given the foregoing, it is of interest to examine the effect of mutation at position 34 (*Rb. capsulatus* numbering) or 29 (vertebrate cytochrome *c* numbering). As with proline at positions 35/30, glycine is highly conserved at position 34/29 and is adjacent to the proline. Moreover, the imidazole of the ligated histidine is adjacent to Gly 34/29 in the folded protein, and a hydrogen bond between the NH of Gly 34 and the CO of Cys 16 (*Rb. capsulatus* cytochrome c_2 numbering) is highly conserved among the cytochromes *c* (*11*−*14*). In yeast cytochrome *c*, the mutation of glycine to serine at this position results in a nonfunctional (in vivo) cytochrome *c* which is present at 70% of the level of wild-type (*15*). To date, Gly 29 mutants of eukaryotic cytochrome *c* have not been characterized, although the lack of in vivo function suggests alterations sufficient to inhibit the interaction with the oxidase, reductase, or both. To explore the role of the conserved glycine at position 34 in *Rb. capsulatus* cytochrome c_2 and more generally to obtain a better understanding of the structural region defined by Gly 34, Pro 35, and the ligated histidine, we are reporting here on the mutation of *Rb. capsulatus* cytochrome c_2 glycine 34 to serine.

In this paper, three types of NMR data will be presented for comparison of the G34S, P35A, and wild-type cytochromes c_2: first, chemical shift differences between the wild-type and mutants in each redox state is used to identify regions where the mutant structure differs from the wild-type structure; second, a comparison of the calculated pseudocontact shift and the observed paramagnetic shift for the wild-type and the mutants defines the regions where the redox-dependent structural changes occur for wild-type and mutant; and finally, the differences in NOE patterns between the wild-type and the mutant G34S in the two redox states reflect significant local adjustments in structure. The NOE and chemical shift evaluations do not necessarily give overlapping results since the NOE is a direct measure of the amount of interaction between two protons, whereas the chemical shift is a measure of the change in the magnetic environment which would result from structural changes at, or nearby, the proton.

For the analysis to be presented, data for both redox states of the cytochrome c_2 G34S mutant is reported. In this context, it is important to note that the solution structure of the reduced *Rb. capsulatus* cytochrome c_2 (*16*) has been shown to be essentially the same as the crystal structure. A number of studies of both *Rb. capsulatus* cytochrome c_2 wild-type and mutants have shown that there are no major structural changes from that of the wild-type for either oxidation state (*6*, *8*, *16*−*19*; Zhao, unpublished data). This is consistent with other observations that solution structures have only localized structural differences between the two oxidation states, for example, horse cytochrome *c* (*20*−*23*) and *Saccharomyces cerevisiae* cytochrome *c* (*24*, *25*).

MATERIALS AND METHODS

Protein purification and sample preparation for mutants G34S and P35A were as previously described (*26*). The *Rb. capsulatus* G34S and P35A mutants were expressed on plasmids in a cytochrome c_2 minus strain of *Rb. sphaeroides* (Gadc2), which is unable to support photosynthesis in the absence of cytochrome c_2 (*26*). On the basis of colony size,

Table 1: Properties of *Rb. capsulatus* Cytochrome c_2 Wild-Type and Mutants

cytochrome c_2	$E_{m,7}$ (mV)[a]	$\Delta\Delta G_{redox}$ (kcal/mol)	pK_{695}[b]	$\Delta\Delta G_{695}$ (kcal/mol)	C_m (M)[c]	$\Delta\Delta G_u$[d] (kcal/mol)
wild-type	367		8.90		1.54	
P35A	358	+0.2	8.90	0.0	0.90	+2.0
G34S	330	+0.9	8.60	+0.7	0.86	+2.2

[a] Midpoint oxidation−reduction potential at pH 7.0 (vs SHE). $E_{m,7}$ values are reproducible to ±3 mV or ±0.07 kcal/mol. [b] Determined from the effect of pH on the 695 nm absorbance band. pK values are ±0.2 pH units or ±0.3 kcal/mol. [c] Conformational stability to guanidine-HCl denaturation for the oxidized cytochrome, given as the concentration of Gdn-HCl (in 20 mM Tris, pH 7.5) required for 50% denaturation (±0.05 M). [d] The relative stability to denaturation (guanidine-HCl) in free energy terms (*27*). Measurements are reproducible to ±0.3 kcal/mol.

the *Rb. capsulatus* merodiploids (for G34S and P35A) supported growth to almost the same extent as did wild-type cytochrome c_2 from both *Rb. sphaeroides* and *Rb. capsulatus* (*26*; this work). Moreover, cytochrome c_2 yields were comparable in all cases. The methods for optical spectroscopy, oxidation−reduction potential determination, and the thermodynamics of guanidine hydrochloride (Gdn-HCl) denaturation have been previously reported (*27*). Determination of the alkaline transition pK_{695} was performed as in Caffrey and Cusanovich (*28*).

NMR spectra for both cytochrome c_2 redox states were acquired on a Bruker AM 500 spectrometer at pH 6.0 and 30 °C. Conventional 2D experimental pulse sequences of DQF-COSY (*29*), TOCSY (*30*, *31*), and NOESY (*32*, *33*) were utilized for data collection. 2D ^{1}H spectra were usually acquired with a spectral width of 10 kHz, 900 t_1 points, 2048 data points in t_2, and 128 transients for each t_1 point. NOESY spectra were recorded with mixing times of 50 and 100 ms, and TOCSY spectra were recorded with a mixing time of 60 ms. All 2D spectra were processed on a Silicon Graphics work station with FELIX software (Molecular Simulations).

For the two cytochrome c_2 oxidation states, the observed chemical shift difference for individual protons include the Fermi contact and pseudocontact contributions, as a consequence of the paramagnetic iron in the oxidized protein, as well as any diamagnetic contribution due to structural changes (*19*, *34*) and can be described by eq 1:

$$\Delta\text{obs} = \delta_{ox} - \delta_{red} = \Delta c + \Delta\text{pc,x} + \Delta s \qquad (1)$$

where δ_{ox} and δ_{red} are the measured chemical shifts for the two oxidation states, Δc is the Fermi contact contribution to the chemical shift, Δpc,x is the pseudocontact contribution, and Δs is the diamagnetic chemical shift that is due to any structural change resulting from a change in redox state. The Fermi contact paramagnetic shift is a "through bond" contribution and is due to the presence of unpaired spin density at each proton (or other nucleus) in the molecule (*35*, *36*). It is limited to protons on the heme and the ligated methionine and histidine residues due to the rapid attenuation with an increase in the number of intervening bonds; the pseudocontact shift is a "through space" dipolar effect and depends on the position of the nucleus with respect to the heme unpaired electron. Because of the decrease of the Fermi contact contribution with the number of intervening bonds, Δc is zero for all residues that are not directly attached to the heme. The calculation of the optimized **g**-tensor and the pseudocontact shifts for the G34S and P35A mutant proteins were made using the hyperfine shift data, $\delta_{ox} - \delta_{red}$, and the proton coordinates from the crystal structure of the reduced wild-type protein (*37*) as previously described (*19*, *34*).

RESULTS AND DISCUSSION

Basic Chemical Properties of G34S. Table 1 compares the oxidation−reduction potential, alkaline pK_{695}, and the conformational stability from Gdn-HCl denaturation studies for wild-type and the P35A and G34S mutants. The data are presented in terms of both the parameter measured and the difference in free energy ($\Delta\Delta G$) between the mutant and wild-type. For $\Delta\Delta G$, the convention used is that a positive value [for example, $\Delta\Delta G_u$ which is given as $\Delta G_{u(WT)} - \Delta G_{u(mutant)}$] indicates that the mutant is less stable than the wild-type (see ref *3* for details).

The pK of the 695 nm transition [pK_{695} (*10*, *38*)] for G34S is 0.3 pH units lower than the wild-type and the P35A mutant (Table 1). Thus, it appears that the heme iron−methionyl sulfur coordinate bond is affected to a small extent by the G34S mutation but not the P35A mutation. Oxidized G34S is substantially less stable as measured by Gdn-HCl denaturation than wild-type (approximately 2.2 kcal/mol less stable) but not significantly different from the P35A mutation (Table 1). We assume that the denatured states for the wild-type cytochrome and mutants are the same or similar. Thus, we conclude that oxidized G34S is significantly destabilized relative to wild-type (approximately 45% of the total free energy for folding) but much less so in terms of the iron−sulfur coordination bond where it is destabilized by only 0.4 kcal/mol. In contrast, the redox potential of G34S is substantially less (by 37 mV) than wild-type and also significantly less (by 28 mV) than P35A. Given that the stability of oxidized G34S is essentially that of P35A (Table 1), the redox potential data suggest that the reduced state of G34S is significantly more destabilized by the mutation than the oxidized state. In the limit, if there is no difference in the redox potential between wild-type and the mutant, the difference in stability between the oxidized and reduced forms of the mutant and the wild-type would be the same. Similarly, if the redox potential is less positive in the mutant (assuming the oxidized stabilities are the same), the reduced form must have been destabilized relative to the oxidized form by an amount equivalent to the change in redox potential ($\Delta\Delta G_{redox} = -nF\Delta E_0'$) (*3*). Thus, in the case of P35A, with an E_0' of 358 mV, the reduced form must have been destabilized 2.2 kcal/mol compared to wild-type while the oxidized form was destabilized 2.0 kcal/mol. Similarly, in the case of G34S, the reduced form must have been destabilized 3.1 kcal/mol relative to wild-type while the oxidized form was destabilized only by 2.2 kcal/mol. Given the foregoing, the oxidized forms of P35A and G34S are

destabilized to roughly the same extent relative to wild-type, while the reduced form of G34S is destabilized to a significantly greater extent (approximately 0.9 kcal/mol); however, the reduced form remains substantially more stable than the oxidized form, hence the relatively high redox potential (330 mV). Alternatively, the changes in relative stability of the two redox states could be viewed in the context of differential effects of the mutation on the association constant for the binding of the axial ligands in the two redox states.

Backbone Conformational Differences between Wild-Type and G34S. The complete assignments of the ^{1}H NMR spectra of G34S cytochrome c_2 for both redox states were accomplished by a combination of TOCSY, DQF-COSY, and NOESY experiments using the technique of sequential assignment (*39*). The assignment data are available as Supporting Information. Overall, the short-range NOEs used to sequentially connect residues suggest that the secondary structure for reduced and oxidized forms of G34S is essentially the same and similar to the respective oxidation state of wild-type cytochrome c_2, except near the site of mutation. For example, a short-range NOE between the αH of Cys 16 and the NH of His 17 was observed in the wild-type protein, but not in the G34S protein. In contrast, an NOE between the αH of Thr 15 and the NH of Cys 16 was observed in G34S but is absent in the wild-type protein, suggesting that the segment of backbone from Thr 15 to His 17 is rotated in the mutant, leading to an increase in stability.

The differences in the NH and αH chemical shifts between the G34S and wild-type (*40*; Zhao, unpublished data) for the reduced and the oxidized forms (excluding residue 34) are shown in Figure 2. Strikingly, there are four regions of significant chemical shift differences (>0.05 ppm) between wild-type and G34S for the reduced cytochromes (Figure 2A). These regions (16−19, 27−38, 46−56, and 94−98, the latter three regions are highlighted in Figure 1) do not correlate with regions of defined secondary structure (i.e., are not in helical regions) except for Ser 56. Studies with yeast cytochrome *c* have identified three or four (depending on how the structural regions are viewed) Ω loops which encompass the sequence regions 78−100, 41−69 (or 41−50 and 45−69 if divided into two Ω loops), and 17−37 using cytochrome c_2 numbering (*40*−*42*). Note that the cytochrome c_2 Ω loops are larger than with the yeast cytochrome because of insertions. The Ω loops have been treated as cooperative folding units (*42*) or subdomains (*43*) based on H/D exchange and NMR studies. In terms of stability to denaturation, with yeast cytochrome *c*, the Ω loops have the order (using cytochrome c_2 numbering) 78−100 < 41−69 < 19−40 (*41*). The cytochrome c_2 domains perturbed by the G34S mutation are in Ω loop regions. Three of the perturbed regions (16−19, 27−36, and 46−56) are proximal to the site of mutation in the folded protein, and these chemical shift differences must, in part, be due to the short-range effects of the replacement of glycine by serine. Interestingly, the region 94−98, which is located on the opposite side of the heme, is perturbed in the reduced G34S mutant, but not in the P35A mutant (*8*). The effect of the mutation in this region apparently has been propagated through elements of the secondary structure (Ω loops), possibly as a result of the perturbation of hydrogen bond networks, as discussed below.

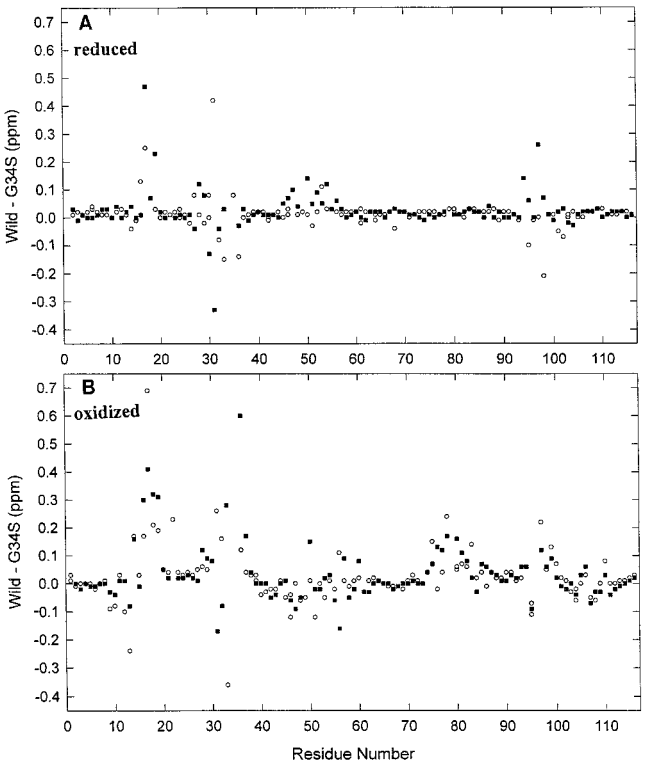

FIGURE 2: Differences in chemical shifts for the αH (○) and NH (■) protons of wild-type and G34S for reduced (A) and oxidized (B) cytochrome c_2 from NMR spectra recorded at 30 °C and pH 6.0. The accuracy of the chemical shift is 0.01 ppm. The chemical shifts for αH and NH of wild-type protein are taken from ref *43* for the reduced form and Zhao (unpublished data) for the oxidized form.

The difference in chemical shifts between oxidized G34S and wild-type is similar to those observed with the reduced protein, with the regions 10−19, 27−30, 46−56, 72−80, and 94−98 clearly affected by the mutation. However, several differences are evident. First, approximately 40 additional protons have chemical shifts that are significantly different (>0.05 ppm) from wild-type in the oxidized protein, as compared to the reduced state. These additional significant chemical shifts presumably result from the substantially reduced stability of the oxidized protein relative to the reduced state as reflected in the Δ*s* term in eq 1. The presence of the paramagnetic iron affects the chemical shift of residues near the heme (Δpc,x in eq 1); further, the two heme axial ligands have contributions from the Fermi contact term (Δ*c*, eq 1). Second, the majority of the additional significant changes in chemical shift occur in two regions: (1) 16 αH and NH protons are significantly perturbed in the 10−19 region for the oxidized protein as compared to 5 for the reduced; (2) 16 αH and NH protons are perturbed in the oxidized mutant in the region 72−80, a region where no significant perturbations are observed in the reduced protein (Figure 2). Clearly, some of these differences between the oxidized and reduced states of the wild-type and G34S mutant proteins could result from changes in the pseudocontact chemical shifts which are due to the paramagnetic iron in the ferricytochrome (see below).

Analysis of the Heme and Heme−Ligand Environment. The chemical shifts for the assigned resonances of the heme and proximal side chains for both the wild-type (*8*) and G34S proteins in the reduced state are given in the Supporting

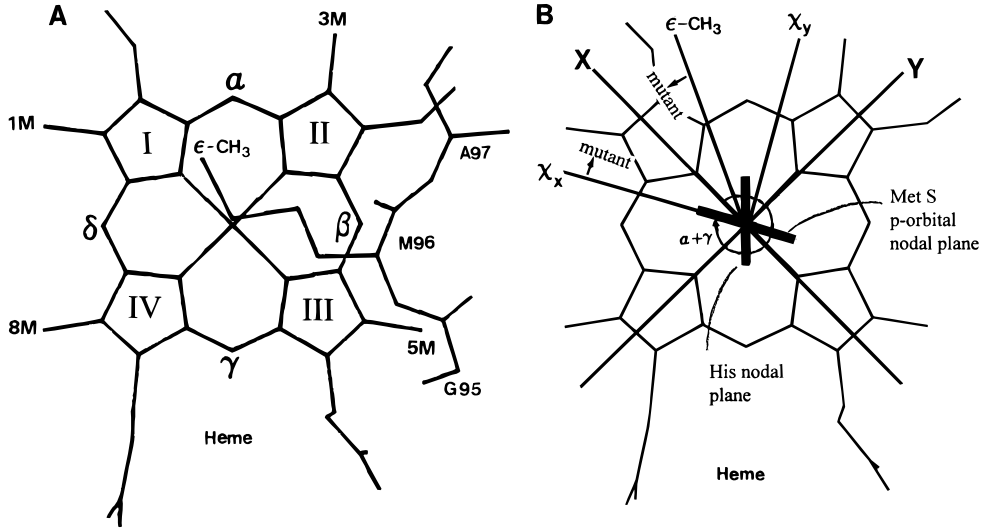

FIGURE 3: (A) *Rb. capsulatus* cytochrome c_2 heme and methionine 96 ligand (on the top) from the crystal coordinates (*37*). The distances from the ϵ-methyl of methionine to the α- and δ-mesos of the heme are 3.76 and 4.06 Å, respectively, in the crystal structure. (B) Heme group and **g**-tensor system. The *x*- and *y*-axes of the heme-based coordinate system, viewed from Met-96, are indicated. The *x*- and *y*-axes of the **g**-tensor for G34S are rotated about the principal axis in the clockwise direction as compared to that of the wild-type since $\alpha + \gamma = 343°$ for wild-type, while $\alpha + \gamma = 349°$ for G34S. The ϵ methyl of Met 96 is rotated in the counterclockwise direction.

Information (the assignment process for the oxidized G34S heme is still in progress). The majority of the heme proton chemical shift differences are less than experimental error (±0.01 ppm), indicating that the heme environments in G34S and wild-type are generally similar. However, the chemical shifts for the β-meso and methyl-5 of the heme are substantially perturbed in the G34S mutant relative to wild-type (−0.13 and 0.06 ppm, respectively), a result which was not obtained with the P35A mutant (*8*). It appears likely that a structural rearrangement near the β-meso and methyl-5 protons has occurred as a result of the larger serine side chain protruding in the direction of the front edge of the heme (Figure 1).

Significant differences in the chemical shifts for the protons of propionate-6 and to a lesser extent propionate-7 are found between the reduced wild-type and G34S cytochromes (0.1 and −0.1 ppm for the propionate 6α protons and 0.07 and −0.01 ppm for the propionate 7 α protons) where propionate-6 is the front heme propionate and propionate-7 the rear heme propionate (Figure 1). These results are similar to those found for the P35A mutant (*8*) and suggest that changes occur in the environment of these propionates. The time-averaged ring current effects of Phe 51 and Tyr 53, which are proximal to propionate-6 in the folded protein, differ since they have significantly increased flip rates in G34S, increasing from intermediate to fast for Phe 51 and from a slow to intermediate rate for Tyr 53, compared to the wild-type protein (*43*). Changes in the ring current effects of these aromatic substituents may, in part, account for the chemical shift differences of propionate-6. In addition, the ϵNH of Arg 43, the N_πH of His 17, and the N(1)H of Trp 67 are significantly perturbed in the mutant relative to the wild-type cytochrome. The crystal structure of *Rb. capsulatus* cytochrome c_2 (*37*) has the ϵNH of Arg 43 and the N(1)H of Trp 67 hydrogen bonded to propionate-7 and the N_πH of His 17 is located near the site of mutation. Thus, these shifts suggest that the micro-environment of N_πH of His 17, ϵNH of Arg 43, and N(1)H of Trp 67 are altered in G34S due to the mutation. Moreover, perturbation of the γH of Met 96 is found (−0.04 ppm), which is apparently sufficient to be reflected in a small change in the alkaline pK_{695}. Arg 43 is hydrogen bonded to a bound water (18H in the crystal structure) as well as to propionate-7. Moreover, Trp 67 is hydrogen-bonded to the same water as well as to the Arg 43 carbonyl oxygen. Thus, it appears that the Ser 34 substitution also perturbs propionate-7 and the related hydrogen bond network.

NOE Differences between Wild-Type and G34S in the Reduced State. In general, the NOE data for those protons, which exhibit large differences in chemical shifts, should indicate structural changes related to differences in the heme environment and stability between the wild-type and G34S. However, we find that a comparison of short-range and long-range NOEs between the reduced wild-type and the G34S mutant does not indicate obvious differences in the NOE patterns except for a few segments near the mutation site, for example, the segment of residues 15−17, as discussed above. This suggests that the secondary and tertiary structures are similar for both cytochromes and also indicates that, in general, the chemical shifts are substantially more sensitive than the NOE data in identifying structural changes in solution.

The NOE connectivities can be used to indicate the orientation of the ϵ methyl of Met 96 and the heme protons. For the wild-type cytochrome c_2, a NOE was observed from the ϵ methyl of Met 96 to the heme α-meso proton, but not to the δ-meso proton. This is consistent with the crystal structure of the wild-type protein (*37*) where the ϵ methyl is closer to the heme α-meso proton than the δ-meso proton (Figure 3A). For the G34S mutant, NOEs were observed from the ϵ methyl of Met 96 to both the α- and δ-meso protons. Thus, it appears that the time averaged orientation of the ϵ methyl of methionine 96 is rotated away from the α-meso toward the δ-meso in the G34S mutant as compared to the position in wild-type cytochrome crystal structure as shown in Figure 3A.

The C(2)H, C(5)H, and N_πH (labeled CE1, CD2, and ND1, respectively, in the crystal structure) of His 17 exhibit

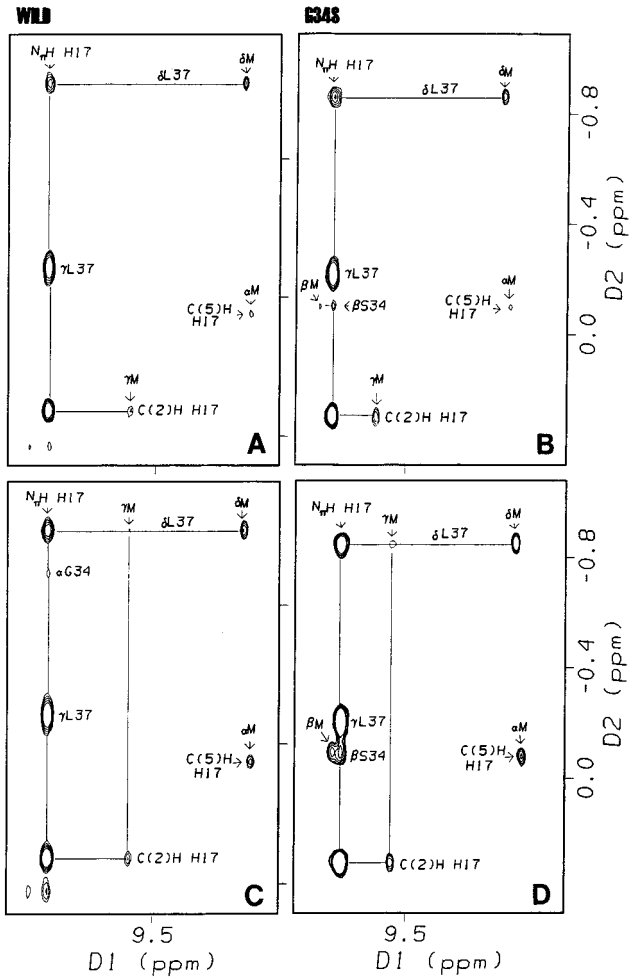

FIGURE 4: Sections of NOESY spectra of (A) wild-type and (B) G34S with a mixing-time of 50 ms and (C) wild-type and (D) G34S with a mixing time of 100 ms for ferrocytochrome c_2 recorded at 30 °C and pH 6.0. In the spectra of G34S (B and D), long-range NOEs from the β proton of Ser 34 to the $N_\pi H$ of His17 and β-meso protons are shown. In addition the long-range NOE between the α proton of Gly 34 and the $N_\pi H$ of His 17 is observed in the wild-type spectrum with a mixing-time of 100 ms (C). The long-range NOE between the C(2)H of His 17 and the γ-meso proton of the heme in G34S (B) is stronger than that in the wild-type (A).

large differences in chemical shifts between the reduced wild-type and the reduced G34S mutant (0.07, 0.11, and 0.10 ppm, respectively), likely a result of a direct effect of the mutation, since the imidazole ring of His 17 is adjacent to residue 34 in the folded protein and there are hydrogen bonds between the NH of Gly 34 to the CO of Cys16 and the $N_\pi H$ of His 17 to the CO of Pro 35 (Figure 1). The NOE peak assigned to the connectivity of C(2)H of His 17 and the γ-meso of heme is weak for the wild-type protein in the NOESY spectrum with a mixing time of 50 ms (Figure 4A), while the equivalent peak for G34S (Figure 4B) is significantly stronger in the NOESY spectrum under the same experimental conditions. These differences in NOE intensities between wild-type and G34S suggest that the C(2)H of His 17 is closer to the γ-meso proton in G34S than in wild-type due to a perturbation by the larger side chain of Ser 34. This could result from either rotation about the Fe−N bond or a tipping of the imidazole off-axis toward the γ-meso proton.

A weak peak from the αH of Gly 34 to $N_\pi H$ of His 17 was found in the NOESY spectrum with a mixing time of 100 ms for the reduced wild-type cytochrome (Figure 4C). However, for the G34S mutant, there were strong peaks between the β protons of Ser 34 to the $N_\pi H$ of His 17 and the β-meso proton of the heme in the NOESY spectrum under the same experimental conditions (Figure 4D). These observations suggest that serine 34 extends its side chain toward the β-meso proton of the heme (Figure 1), so that the front edge of the heme ring is influenced by the intrusion of the side chain of the mutant. In addition, G34S has a strong NOE between a Ser 34 β proton (data not shown) and the methyl-5 protons. However, no NOE between the Ser 34 α proton and the heme was observed. These results are consistent with the chemical shift data where the β-meso and methyl-5 protons are affected by the mutation. The substitution of Ser and the resulting interaction with the β-meso proton may alter the hydrophobicity in the heme environment, stabilizing the oxidized state relative to the reduced and thus contributing to the lower redox potential.

Table 2: **g**-Tensor Parameters for the Wild-Type and Mutants of *Rb. capsulatus* Cytochrome c_2

protein	Δg_{ax}^2 [a]	Δg_{eq}^2 [a]	α (deg)[b]	β (deg)[b]	γ (deg)[b]	$\alpha+\gamma$ (deg)	χ^2/N
wt	4.80	−1.00	152	12	191	343	0.001
P35A	4.10	−0.90	156	12	192	348	0.001
G34S	4.40	−1.10	149	15	200	349	0.001

[a] Δg_{ax}^2, Δg_{eq}^2 are the axial and equatorial anisotropies of the **g**-tensor, $\Delta g_{ax}^2 = g_{zz}^2 - 1/2(g_{xx}^2 + g_{yy}^2)$ and $\Delta g_{eq}^2 = g_{xx}^2 - g_{yy}^2$. [b] α, β, and γ are the Euler angles that define the orientation of the **g**-tensor principal axis system relative to the heme coordinate system; χ^2/N expresses the precision for the least-squares fitting where $\chi^2 = \Sigma(\Delta\text{obs} - \Delta\text{pc,x})^2$ and N is the number of residues (*19*).

Redox Conformational Differences between Reduced and Oxidized G34S. The optimized **g**-tensor anisotropies for the oxidized form of G34S and P35A were obtained from a set of selected NH proton chemical shifts using a least-squares fitting procedure, as previously described (*19*, *34*). The calculation of the **g**-tensors for both the wild-type and G34S proteins is based on the reduced crystal structure (*37*) since, as previously discussed, the solution structure for both cytochromes (and both redox states) appear to be the same and are essentially the same as the crystal structure with only small localized structural changes. These optimized **g**-tensor anisotropies along with those of the wild-type (*19*) are given in Table 2 The observed paramagnetic shifts were obtained from the assignment data for the oxidized and reduced cytochromes. The calculated pseudocontact shifts (Δpc,x) were obtained from eq 1 using the optimized **g**-tensor anisotropies (Table 2) and the coordinates of the reduced wild-type protein (*37*).

In Table 2, the orientation of the **g**-tensors for the wild-type and G34S is given in terms of the Euler angles α, β, and γ that define the principal axes (g_x, g_y, and g_z) relative to the heme coordinate system (*19*, *34*). For the orientation of the **g**-tensors for the wild-type and G34S proteins, a comparison can be made between the values of $\alpha + \gamma$ [which is representative of the rotation of the orthogonal g_x and g_y axes relative to the heme x and y axes (*34*) when β is small as observed here]. For the G34S mutant, $\alpha + \gamma = 349°$, and for the wild-type protein, $\alpha + \gamma = 343°$, which represents a clockwise rotation of 6° about the heme center (Figure 3B) when comparing the change of the **g**-tensor upon

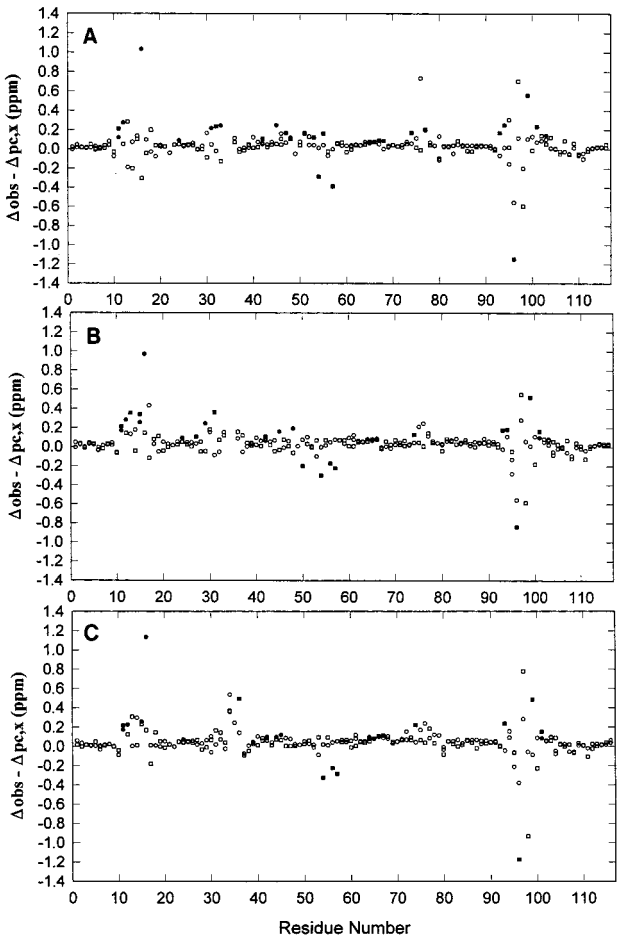

FIGURE 5: Differences between the observed paramagnetic shift and calculated dipolar shift (observed − calculated) for backbone amide protons (open squares) and α protons (open circles) as a function of the residue number for G34S (A), P35A (B), and wild-type (C) proteins. Protons selected by eq 8 from ref *19* are labeled for amide protons (filled squares) and for α protons (filled circles) and appear to have undergone significant redox-related conformational changes with the change in oxidation state.

mutation. For the G34S and wild-type proteins, the change in the orientation of the ligated methionine ϵ-methyl side chain and the **g**-tensor occurs in the opposite direction about the center of the heme (Figure 3B). These changes are consistent with the observation that the **g**-tensor (that is, the magnetic axes) and the axial ligand plane or the methionine p_π rotate in the opposite direction for low-spin ferriheme proteins when there is a change in the orientation of an axial ligand due to a mutation (*44*, *45*).

To assess the redox-coupled conformational changes, a comparison was made between the observed paramagnetic shifts and the calculated pseudocontact shifts (from the optimized **g**-tensor and the crystal structure of the reduced protein) for oxidized G34S for both the backbone NH and αH protons as a function of residue number, as shown in Figure 5A. For comparison, the results for P35A and wild-type proteins (*19*) are shown in Figure 5, panels B and C, respectively. Residues which show a significant difference between the observed and calculated pseudocontact shift were selected, as previously described (*19*) and are shown as solid symbols in Figure 5. The coordinates of ferrocytochrome c_2 (*37*) were used in the calculation of the pseudocontact shifts for the wild-type and mutant proteins. Thus, the significant differences between the observed and calculated shifts presumably result from structural changes on oxidation (or changes in dynamics which result in different time averaged position), since both the NH and αH protons, even of His 17 and Met 96, are too many bonds away from the paramagnetic iron for any contact shift. As previously discussed, the overall solution structures are the same for the two oxidation states of wild-type cytochrome, and for the mutants which have been studied, it has been shown that there are no major structural changes as compared to wild-type (*6*, *8*, *16*−*19*, Zhao, unpublished data). The relatively small localized changes which are observed with a change in oxidation state must be significant in poising the redox potential through modulation of the relative stability of the two redox states and/or the affinity of the axial ligands.

In the case of G34S (Figure 5A), main-chain protons (αH, NH) from residues 11, 12, 16, 24, 31−33, 42, 45−48, 51, 53−55, 57, 64−68, 74, 77, 80, 93−96, 99, 101, and 103 appear to exhibit significant conformational changes resulting from oxidation. Many of the residues which appear to exhibit significant structural changes in G34S (Figure 5A) are the same as those altered by oxidation of the wild-type protein [Figure 5C (*19*)]. However, residues 31−33, 47−48, 51, and 53, which are proximal to the site of the G34S mutation in the tertiary structure, as well as residues 77, 80, and 94, which are on the opposite side of the heme, exhibit significant redox conformational differences which are not observed in the wild-type protein. As a consequence, it appears that the backbone for residues 31−33, adjacent to 34, is altered due to the effects of the mutation and the 47−53 region, which is spatially close to the mutation position in the folded protein (*37*), is also apparently perturbed. However, it is possible that changes in ring current effects of Phe 51 and Tyr 53 may also contribute to the observed differences in the 47−53 region (*8*).

Some of the redox-coupled structural changes are undoubtedly the result of a change in the hydrogen bond network that involves the internal water molecules (labeled 31H, 43H, 18H, and 45H) (*37*). Propionate-7 is hydrogen bonded to an internal water molecule (18H), which, in turn, is within H-bond distance with Thr 47, Tyr 48, and Tyr 53 (*37*). Changes at the heme propionate-7 could affect the 47−53 region, or conversely, changes in the 47−53 region could contribute to a change in propionate-7. The changes which occur on the opposite side of the heme from the mutation could result from the perturbations which occur in the heme and the propionates (Table 2) due to the intrusion of the serine 34 side chain. Any change which occurs in propionate-6 could affect Thr 94 because of the hydrogen-bonding network with propionate-6, an internal water molecule (43H), and Thr 94 (*37*). Propionate-6 is also involved in internal water hydrogen bonds with Lys 54 (internal water 45H) and Ile 57 (internal water 43H), a region which exhibits a larger overall redox effect for the G34S mutant than for the wild-type protein.

However, it appears that a localized increase in stability on oxidation can occur in some structural regions, even though there is an overall decrease in stability. For example, the backbone of residues 15−17 has different NOE connectivities in G34S with respect to wild-type, and the αH of Thr 15 undergoes a significant conformational change on oxidation in the wild-type protein (Figure 5C), that is not

observed in the G34S (Figure 5A), consistent with a stabilization in the region of residues 15−17 for G34S. Moreover, coupled structural changes occur in the wild-type protein on oxidation that are not observed in the G34S mutant. For example, the αH of Gly 34 and NH of Asn 36 undergo significant conformational changes on oxidation of the wild-type, but the G34S mutation disrupts this region in the reduced state (destabilizes G34S) so that on oxidation of G34S there are no observed changes in this region.

Comparison of Mutants G34S and P35A. The G34S and P35A mutations, given their proximity in the structure, should have some features in common that bear on the importance of their structural domain in ligation and overall stability. However, because of the differences in both size and hydrophobicity, as well as their structural roles, the effects of the mutations studied should also have distinguishing features. The significant redox conformation changes for P35A (Figure 5B) are generally similar to those found with G34S (Figure 5A) with protons from residues 11−13, 15, 16, 24, 27, 29, 31, 42, 45, 46, 48, 50, 54, 56−57, 61, 64−66, 74, 93−96, 99, 101, 103, and 104 having significant conformational changes on oxidation. Residues 27, 29, 31 and 48, and 50, which are close to the site of the P35A mutation, exhibit significant redox conformational changes which are not observed in the wild-type cytochrome. Both of these regions for P35A, 27−31 and 48−50, are coincident with regions 28−36 and 46−54, which have been shown to have substantive chemical shift differences between the reduced wild-type and reduced P35A cytochrome c_2 (*8*) as well as between G34S and wild-type as discussed above.

Residues 13 and 15 exhibit significant redox conformational changes in the P35A mutant, which are not observed in the G34S mutant; for this region in wild-type, a change is observed at residue 15, but not 13. This is consistent with an increase in the stability of segment 15−17 in G34S (while the overall stability is decreased in other regions), based on the NOE connectivities, as discussed above, but the mutation in P35A appears to decrease the stability for segment 13−15 as reflected by the chemical shift and **g**-tensor calculations. The NH proton of Lys 14 has a chemical shift difference (reduced cytochrome) of more than 0.5 ppm between the wild-type and P35A cytochromes (*8*), which is consistent with the redox conformational changes in the segment 13−15 for P35A but which is not observed in G34S.

CONCLUSIONS

The G34S mutant has the same basic secondary structure as wild-type cytochrome c_2 and appears to be fully functional in vivo. Nevertheless, substantial changes in the structure/chemical environment of specific amino acid positions do occur. These can result from the repositioning of side chain and/or backbone or from changes in the internal dynamics which result in new time-averaged positions. These perturbations resulting from the mutation can result in local stabilization or destabilization, depending on the residue position, although the overall impact is a significant destabilization of the folded structure. It appears that substitution of serine at position 34 results in a perturbation of the heme β-meso and the methyl-5 protons and that the corresponding adjustments of the backbone and side chains propagate through hydrogen bond networks and alter interactions in defined regions. The structural regions affected, 10−19, 27−38, 46−56, and 94−98 in the reduced mutant, and with the addition of the region 72−80 in the oxidized protein, have a number of features which logically couple the mutation with the observed perturbations. Thus, the ligated histidine at position 17 and adjacent amino acids interact strongly with Gly 30, Ala 31, Lys 32, Thr 33, Gly 34, Pro 35, and Leu 37, clearly a set of interactions which would be altered by the mutation at position 34, discussed here, or at Pro 35, analyzed in earlier studies (*8*). In addition, the rear heme propionate (propionate-7) is involved in a network of interactions involving the bound water 18H and amino acids, including Gly 42, Arg 43, Thr 44, Gly 46, Thr 47, Tyr 48, Tyr 53, and Trp 67, and which is coupled to the 30's region through hydrogen bonds between Asn 36 and Arg 43. Finally, hydrogen bonds involving the front heme propionate (propionate-6), three bound waters (31H, 43H, and 45H), and the amino acids in positions 54, 56, 57, 75, and 94−96 define a third general area, which is perturbed and which couples the 46−56 region to the 94−98 region, as well as involving Tyr 75. The effect of the mutation at position 34, discussed here, is generally similar to those found for the P35A mutation, with the exception of the 94−98 region, which is not affected in reduced P35A. Presumably, the P35A mutation does not sufficiently alter the front heme propionate hydrogen bond network to propagate the destabilization to the 94−98 region. It is notable that the regions perturbed by the G34S mutation in the reduced protein are the same general areas that are affected by oxidation of the wild-type cytochrome. Taken together, the results presented here clearly demonstrate the importance of the bound waters, the interactions mediated by the propionates, the interactions proximal to and involving the ligated histidine, and the apparent 6° change in the methionine orientation. It is anticipated that further studies should elucidate the most critical components of the structural regions, discussed here, and assist in defining in specific terms the features responsible for the stability of the cytochromes c_2, as well as the control of the redox potential, as modulated through the relative stability of the two redox states.

SUPPORTING INFORMATION AVAILABLE

Two tables giving the chemical shifts for ferri and ferro G34S. This material is available free of charge via the Internet at http://pubs.acs.org.

REFERENCES

1. Alber, T. (1989) *Annu. Rev. Biochem. 58*, 765−798.
2. Loll, P. J., and Lattman, E. E. (1990) *Biochemistry 29*, 6866−6873.
3. Caffrey, M. S., and Cusanovich, M. A. (1994) *Biochim. Biophys. Acta 1187*, 277−288.
4. Meyer, T. E., and Kamen, M. D. (1982) *Adv. Protein Chem. 35*, 105−212.
5. Meyer, T. E., and Cusanovich, M. A. (1989) *Biochim. Biophys. Acta 975*, 1−28.
6. Caffrey, M. S., Gooley, P. R., Zhao, D., Meyer, T. E., Cusanovich, M. A., and MacKenzie, N. E. (1997) *Protein Eng. 10*, 77−80.
7. Koshy, T. I., Luntz, T. L., Schejter, A., and Margoliash, E. (1990) *Proc. Natl. Acad. Sci. U.S.A.* 87, 8697−8701.
8. Gooley, P. R., Caffrey, M. S., Cusanovich, M. A., and MacKenzie, N. E., (1991) *Eur. J. Biochem. 196*, 653−661.

9. Koshy, T. I., Luntz, T., Plotkin, B., Schejter, A., and Margoliash, E. (1994) *Biochem. J. 299*, 347−350.
10. Schechter, E., and Saludjian, P. (1967) *Biopolymers 5*, 788−790.
11. Takano, T., and Dickerson, R. E. (1981) *J. Mol. Biol. 153*, 79−94.
12. Bhatia, G. E. (1981) Ph.D. Thesis, University of California, San Diego.
13. Bushnell, G. W., Louie, G. V., and Brayer, G. D. (1990) *J. Mol. Biol. 214*, 585−595.
14. Louie, G. V., and Brayer, G. D. (1990) *J. Mol. Biol. 214*, 527−555.
15. Hampsey, D., Das, G., and Sherman, F. (1986) *J. Biol. Chem. 261*, 3259−3271.
16. Cordier, F., Caffrey, M., Brutscher, B., Cusanovich, M. A., Marion, D., and Blackledge, M. (1998) *J. Mol. Biol. 281*, 341−361.
17. Gooley, P. R., and MacKenzie, N. E. (1990) *FEBS Lett. 260*, 225−228.
18. Gooley, P. R., Caffrey, M. S., Cusanovich, M. A., and MacKenzie, N. E. (1992) *Biochemistry 31*, 443−450.
19. Zhao, D., Hutton, H. M., Cusanovich, M. A., and MacKenzie, N. E. (1996) *Protein Sci. 5*, 1816−1825.
20. Qi, P. X., Di Stefano, D. L., and Wand, A. J. (1994) *Biochemistry 33*, 6408−6417.
21. Qi, P. X., Beckman, R. A., and Wand, A. J. (1996) *Biochemistry 35*, 12275−12286.
22. Banci, L., Bertini, I., Gray, H. B., Luchinat, C., Reddig, T., Rosato, A., and Turano, P. (1997) *Biochemistry 36*, 9867−9877.
23. Banci, L., Bertini, I., Reddig, T., and Turano, P. (1998) *Eur. J. Biochem. 256*, 271−278.
24. Baistrocchi, P., Banci, L., Bertini, I., Turano, P., Bren, K. L., and Gray, H. B. (1996) *Biochemistry 35*, 13788−13796.
25. Banci, L., Bertini, I., Bren, K. B., Gray, H. B., Sompornpisut, P., and Turano, P. (1997) *Biochemistry 36*, 8992−9001.
26. Caffrey, M. S., Davidson, E., Cusanovich, M. A., and Daldal, F. (1991) *Arch. Biochem. Biophys. 292*, 419−426.
27. Caffrey, M. S., Daldal, F., Holden, H., and Cusanovich, M. A. (1991) *Biochemistry 30*, 4119−4125.
28. Caffrey, M. S., and Cusanovich, M. A. (1991) *Biochemistry 30*, 9238−9241.
29. Rance, M., Sorensen, O. W., Bodenhausen, G., Wagner, G., Ernst, R. R., and Wuthrich, K. (1983) *Biochem. Biophys. Res. Commun. 117*, 479−485.
30. Braunschweiler, L., and Ernst, R. R. (1983) *J. Magn. Reson. 53*, 521−528.
31. Davis, D. G., and Bax, A. (1985) *J. Am. Chem. Soc. 107*, 2820−2821.
32. Jeener, J., Meier, B. H., Bachmann, P., and Ernst, R. R. (1979) *J. Chem. Phys. 71*, 4546−4553.
33. Marion, D., and Wuthrich, K. (1983) *Biochem. Biophys. Res. Commun. 113*, 967−974.
34. Feng, Y., Roder, H., and Englander, S. W. (1990) *Biochemistry 29*, 3494−3504.
35. Kurland, R. J., and McGarvey, B. R. (1970) *J. Magn. Reson. 2*, 286−301.
36. Bertini, I., Luchinat, C., Macinai, R., Martinuzzi, S., Pierattelli, R., and Viezzoli, M. S. (1998) *Inorg. Chim. Acta 269*, 125−134.
37. Benning, M. M., Wesenberg, G., Caffrey, M. S., Bartsch, R. G., Meyer, T. E., Cusanovich, M. A., Rayment, I., and Holden, H. M. (1991) *J. Mol. Biol. 220*, 673−685.
38. Pearce, L., Gartner, A., Smith, M., and Mauk, A. (1989) *Biochemistry 28*, 3152−3156.
39. Wüthrich, K. (1986) *NMR of Proteins and Nucleic Acids*, Wiley, New York.
40. Fetrow, J. S., Cardillo, T. S., and Sherman, F. (1989) *Proteins: Struct., Funct., Genet. 6*, 372−381.
41. Bai, T., Sosnick, T. R., Mayne, L., and Englander, S. W. (1995) *Science 269*, 192−197.
42. Fetrow, J. S., Dreher, U., Wiland, D. J., Schaak, D. L., and Boose, T. L., (1998) *Protein Sci. 7*, 994−1005.
43. Gooley, P. R., Caffrey, M. S., Cusanovich, M. A., and MacKenzie, N. E. (1990) *Biochemistry 29*, 2278−2290.
44. Pierattelli, R., Banci, L., and Turner, D. L. (1996) *J. Biol. Inorg. Chem. 1*, 320−329.
45. Shokhirev, N. V., and Walker, F. A. (1998) *J. Am. Chem. Soc. 120*, 981−990.

BI992979A